JOURNAL OF APPLIED ELECTROCHEMISTRY 22 (1992) 28–37

Determination of electrode kinetics by corrosion potential measurements: zinc corrosion by bromine

S. L. CHIU*, J. R. SELMAN

Department of Chemical Engineering, Illinois Institute of Technology, Chicago, Il 60616, USA

Received 5 April 1990; revised 16 May 1990

An attractive way of determining the electrode kinetics of very fast dissolution reactions is that of measuring the corrosion potential in flowing solutions. This study analyses a critical aspect of the corrosion potential method, i.e., the effect of nonuniform corrosion distribution, which is very common in flow systems. The analysis is then applied to experimental data for zinc dissolution by dissolved bromine, obtained at a rotating hemispherical electrode (RHE). It is shown that in this case the current distribution effect is minor. However, the results also indicate that the kinetics of this corrosion system are not of the classical Butler-Volmer type. This is explained by the presence of a chemical reaction path in parallel with the electrochemical path. This unconventional corrosion mechanism is verified by a set of experiments in which zones of zinc deposition and dissolution at a RHE are identified in quantitative agreement with model predictions. The practical implications for the design of zinc/bromine batteries are discussed.

Notation

C_i concentration of species i (mol cm^{-3})
D_i diffusivity of species i (cm^2 s^{-1})
F Faraday constant
i_j current density of species j (A cm^{-2})
i_0^b exchange current density referenced at bulk concentration (A cm^{-2})
J $\dfrac{ZFr_0 i_0^b}{RT\kappa}$, inverse Wa number
N $\dfrac{(1-t_+)}{\Gamma(2/3)\Gamma(1/3)}\left(\dfrac{D_c}{D_{M^{+n}}}\right)^{2/3}\left(\dfrac{C_c^b}{C_{M^{+n}}^b}\right)$
n number of electrons transferred for every dissolved metal atom
P_m Legendre polynomial of order m
r_0 radius of disc, sphere, or hemisphere
s stoichiometric constant
t_+ transference number of metal ion
V_{corr} corrosion overpotential (V)

Greek letters

α anodic transfer coefficient of Reaction 21b
α_a anodic transfer coefficient of metal dissolution
α_c cathodic transfer coefficient of metal dissolution
β anodic transfer coefficient of zinc dissolution
β' velocity derivative at the electrode surface
$\Gamma(x)$ incomplete Gamma function
γ $\dfrac{\partial}{\partial}\left(\dfrac{i_n^b}{C_{M^{+n}}}\right)$, exchange reaction order of M^{+n}
δ $\dfrac{ZFr_0}{\kappa RT}|i_{ave}|$, inverse Wa number
η_a activation overpotential (V)
η_c concentration overpotential (V)
θ polar angle (measured from the pole) (rad)
κ solution conductivity (Ω^{-1} cm^{-1})
ν kinematic viscosity (cm^2 s^{-1})
Φ_0 solution potential at the electrode surface (V)
ω rotation rate (s^{-1})
$*$ indicates dimensionless quantities

1. Introduction

A range of standard electrode kinetic techniques are available to study electrochemical reaction mechanisms [1, 2]. However, the application of these techniques to rapid reactions is frequently complicated by the necessity to make relatively large corrections for ohmic potential drop. To avoid including ohmic potential, several investigators [3–5] have proposed measuring the mixed potential of a corrosion system including the reaction in question. Power and Ritchie [3, 4] used a rotating disc electrode (RDE), to study the dependence of the mixed potential on rotation rate and corrodant concentration in several corrosion or displacement reactions systems, under conditions of kinetic and/or mass transfer control. Scully *et al.* [5], also using a RDE, applied the same concept to study the corrosion of carbon steel in neutral media.

This technique, even though simple, has inherently the following disadvantages: (a) under high rate dis-

* Present address: IBM Corporation, Essex Junction, VTO5452, 10598.

0021-891X/92 $03.00 + .12

solution conditions, the shape of the RDE changes significantly, particularly at the edge of the active area where it is in contact with insulating material. This change of geometry will disturb the distribution of the convective mass transfer rate, especially after prolonged experimentation; and (b) in certain types of flow cells, the effect of ohmic potential drop remains significant. Especially when the primary current distribution is highly non-uniform, as at a RDE, the distribution of corrosion rate may not be uniform as assumed in most analyses [3–5].

To minimize the effect of shape change, Chin [6] proposed the use of a rotating hemispherical electrode (RHE). He calculated the limiting current distribution and the average limiting current by a series expansion method; later Newman [7] presented a more rigorous solution. Nisancioglu and Newman [8] also calculated the current distribution at a rotating sphere below the limiting current. They concluded that, at average current below 68% of the limiting current, the current distribution along the sphere is practically uniform and concentration polarization negligible. The ohmic potential drop may then be approximated by $I/4\pi r\kappa$ or, for a hemisphere, $I/2\pi r\kappa$.

Vahdat and Newman [9] calculated the current distribution of a corroding rotating disc of iron, which exhibits passivation. In their calculations, the ohmic effect was taken into account. However, they did not determine how parameters such as the Wagner number affect the current distribution and, most importantly, the corrosion potential. Therefore, it is not clear within which limits one can make the assumption that the measured mixed potential is free of *IR* effect.

In the first part of this paper, a mathematical model for a corroding rotating metal sphere is formulated. The cathodic reaction is assumed to be mass transfer limited. A parametric study is carried out with special attention to the current distribution at the RHE and the effect of *IR*-drop on corrosion potential. Experimental data are reported for a representative system having rapid corrosion kinetics (Zn/Br_2). These data were fitted to the model with the objective of determining the kinetic parameters of the corrosion reaction, i.e. the exchange current density and anodic transfer coefficient of zinc dissolution. This information is of practical significance due to the role corrosion plays in the charging of zinc/bromine batteries, which are being developed for load-levelling and electric vehicle applications.

The overall reaction in such a battery is

$$Zn(s) + Br_2(aq) \underset{\text{charge}}{\overset{\text{discharge}}{\rightleftharpoons}} Zn^{+2}(aq) + 2Br^-(aq) \tag{1}$$

During the charging cycle, zinc metal is deposited on the negative electrode (NE), while bromine is generated on the positive electrode (PE) and dissolves into the solution. In cells of the design presently used [10], a small part of the bromine in the PE compartment diffuses through the separator and corrodes the NE material, i.e. zinc. The discharge Reaction (1) then takes place in the form of local corrosion, and no electrical work is delivered. This partial self-discharge of the battery not only decreases the overall efficiency, but also affects the micro and macro profiles of the zinc deposit formed at the NE during charge. As the charge–discharge cycles continue, the roughness condition of the surface undergoes continuous change, depending on the history of both the zinc deposition reaction and the zinc corrosion reaction. To understand and model this complex process, the corrosion reaction mechanism and the kinetic rate constants of Reaction 1 must be known.

Conventionally, the overall corrosion Reaction (1) is considered to consist of two electrochemical half reactions:

$$Zn(s) \rightleftharpoons Zn^{+2}(aq) + 2e^- \qquad E_0 = -0.76\,V \tag{2}$$

$$Br_2(aq) + 2e^- \rightleftharpoons 2Br^-(aq) \qquad E_0 = +1.09\,V \tag{3}$$

The exchange of electrons occurs locally on the zinc electrode surface and no net external current is passed through the bulk solution. During discharge of the battery, the large separation of the standard potentials of Reactions 2 and 3 and the fast kinetics of Reaction 3 [11], cause the corrosion rate to be limited by mass transfer of bromine. During charging of the battery, on the other hand, the zinc electrode is under cathodic protection and no corrosion will occur.

Although, as shown by McBeen and Gannon [12], the exposed facets of polycrystalline zinc surface exhibit widely different kinetic rate constants (exchange current densities), the corrosion potential method might be expected to yield information about the average kinetic characteristics of Reactions 2 and 3 under typical conditions. The implications of a mechanism such as that represented by Reactions 2 and 3 are examined in the second part of this paper. It is shown that the experimental evidence suggests an alternative mechanism.

2. Current distribution at a corroding hemisphere

2.1. *Mathematical formulation*

The following formulation applies to two corrosion half reactions, assumed to be:

$$M \rightleftharpoons M^{+n} + ne^- \tag{4}$$

$$sC + ne^- \rightleftharpoons \text{product} \tag{5}$$

For an axisymetric revolving body (Fig. 1), such as a RDE or RHE, the limiting current distribution has been shown by Newman [13] to be

$$i_{\text{lim}} = \frac{\dfrac{nFDC_\infty\sqrt{(\Re\beta')}}{s\Gamma(4/3)}}{\left(9D\int_0^x (\Re/\sqrt{\Re\beta'})\,dx\right)^{1/3}} \tag{6}$$

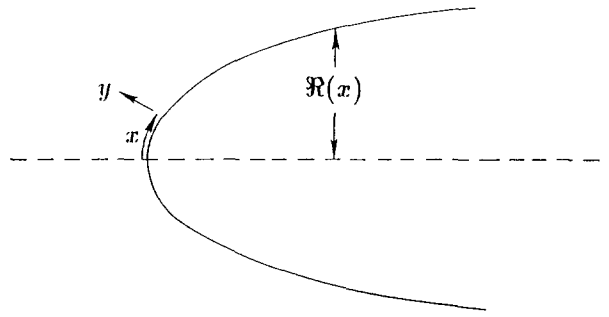

Fig. 1. Schematic of an axisymmetric revolving body.

The local surface concentration may be expressed in terms of the surface flux by a superposition integral:

$$C_0(x) - C_\infty = -\frac{(D/3)^{1/3}}{\Gamma(2/3)} \int_0^x \left.\frac{\partial C}{\partial y}\right|_{y=0,x=x_0} \frac{\Re(x_0)\mathrm{d}x_0}{\left(\int_{x_0}^x \Re\sqrt{(\Re\beta')}\mathrm{d}x\right)^{2/3}} \tag{7}$$

For the RHE [7, 8]

$$\Re = r_0 \sin\theta, \quad x = r_0\theta, \quad \beta' = \nu^{-1/2} r_0 \omega^{3/2} B(\theta)$$
$$B(\theta) = 0.51203\,\theta - 0.1808819\,\theta^3 - 0.040408\sin^3\theta \tag{8}$$

If it is assumed that Reaction 5 is very fast and mass transfer limited, the cathodic current distribution along the sphere can be obtained by substituting Equation 8 into Equation 6:*

$$i_c = -\left(\frac{nFD_c^{2/3} C_c^b \nu^{-1/6} \omega^{1/2}}{s 9^{1/3}\Gamma(4/3)}\right) \times \left(\frac{\sqrt{\sin\theta\, B(\theta)}}{\left(\int_0^\theta \sin\theta \sqrt{\sin\theta\, B(\theta)}\mathrm{d}\theta\right)^{1/3}}\right) \tag{9}$$

By integrating Equation 9 over the sphere, the average limiting current density is [7]:

$$|i_{ave}| = \left(\frac{3^{1/3}(0.417\,077\,5)^{2/3}}{2\Gamma(4/3)}\right)\frac{nF}{s} D_c^{2/3} C_c^b \nu^{-1/6}\omega^{1/2} \tag{10}$$

Equation 10 also determines the average rate at which the metal is dissolving. Normalizing the local current density by Equation 10, the dimensionless current distribution i_c^* is obtained:

$$i_c^* = \frac{i_c}{|i_{ave}|} = \left(\frac{-2}{3(0.417\,077\,5)^{2/3}}\right) \times \left(\frac{\sqrt{\sin\theta\, B(\theta)}}{\left(\int_0^\theta \sin\theta \sqrt{\sin\theta\, B(\theta)}\mathrm{d}\theta\right)^{1/3}}\right) \tag{11}$$

The anodic current density is related to the concentration gradient of M^{+n} at the electrode surface by the condition:

$$i_{M+n} = -\frac{nFD_{M+n}}{(1-t_+)} \left.\frac{\partial C_{M+n}}{\partial y}\right|_{y=0} \tag{12}$$

The net current density is then:

$$i_{net} = i_c + i_{M+n} \tag{13}$$

The solution potential at the electrode surface has been shown to be [8]

$$\Phi_0 = \frac{RT}{ZF}\sum_{m=0}^{\infty} B_m P_{2m}(\cos\theta)$$

where P_{2m} is the Legendre polynomial of order $2m$

$$B_m = \frac{ZFr_0}{\kappa RT}\cdot\frac{4m+1}{2m+1}\cdot\int_0^1 i_{net} P_{2m}(\cos\theta)\mathrm{d}(\cos\theta)$$

$$Z = \begin{cases} \dfrac{n_+ - n_-}{n_+ n_-} & \text{for a single salt;} \\ n & \text{for supported electrolyte.} \end{cases}$$

The dimensionless solution potential at the electrode surface, normalized by RT/ZF, can be expressed in terms of dimensionless net current density i_{net}^*:

$$\Phi_0^* = \sum_{m=0}^{\infty} \delta \cdot \frac{4m+1}{2m+1} \times \int_0^1 i_{net}^* P_{2m}(\cos\theta)\mathrm{d}(\cos\theta)\cdot P_{2m}(\cos\theta) \tag{14}$$

where $\delta = ZFr_0/\kappa RT|i_{ave}|$. The current density i_{M+n} or i_{M+n}^* is not known, but may be assumed to have the form:

$$i_{M+n}^* = -i_c^* f(\theta) \tag{15}$$

Equations 7, 11, 12 and 15 yield the local surface concentration of M^{+n}:

$$\frac{C_{M+n}^s}{C_{M+n}^b} - 1 = N\int_0^y f(y')\frac{\mathrm{d}y'}{y'^{1/3}(y-y')^{2/3}} \tag{16}$$

where $y = \int_0^\theta \sin\theta\sqrt{\sin\theta\, B(\theta)}\mathrm{d}\theta$ and

$$N = \left(\frac{(1-t_+)}{\Gamma(2/3)\Gamma(1/3)}\right)\left(\frac{D_c}{D_{M+n}}\right)^{2/3}\left(\frac{C_c^b}{C_{M+n}^b}\right)$$

Note that the mass transfer parameter N is independent of convection, although it determines the concentration overpotential; δ is the only parameter which depends on the convection rate. The local dimensionless concentration overpotential may now be calculated by substituting Equation 16 into the defining equation [13]:

$$\eta_c^* = \ln\frac{C_{M+n}^s}{C_{M+n}^b} + t_+\left(1 - \frac{C_{M+n}^s}{C_{M+n}^b}\right) \tag{17}$$

The local activation polarization is assumed to satisfy the Butler-Volmer equation

$$i_{M+n} = i_0^b\left(\frac{C_{M+n}^s}{C_{M+n}^b}\right)^\gamma [e^{\alpha_a(nF/RT)\eta_a} - e^{-\alpha_c(nF/RT)\eta_a}]$$

* The minus sign is added to follow the conventional notation, i.e., positive for anodic current and negative for cathodic current.

Table 1. Governing equations for the current distribution at a corroding rotating hemisphere

$$i_c^* = \frac{i_c}{|i_{ave}|} = \left(\frac{-2}{3(0.4170775)^{2/3}}\right)\left(\frac{\sqrt{\sin\theta\, B(\theta)}}{\left(\int_0^\theta \sin\theta \sqrt{\sin\theta\, B(\theta)}\,d\theta\right)^{1/3}}\right) \quad (11)$$

$$i_{M+n}^* = -i_c^* f(\theta) \quad (15)$$

$$i_{net} = i_c + i_{M+n} \quad (13)$$

$$\Phi_0^* = \sum_{m=0}^{\infty} \delta\left(\frac{4m+1}{2m+1}\right)\int_0^1 i_{net}^* P_{2m}(\cos\theta)\,d(\cos\theta)\cdot P_{2m}(\cos\theta) \quad (14)$$

$$\frac{C_{M+n}^s}{C_{M+n}^b} - 1 = N\int_0^y \frac{f(y')}{y'^{1/3}(y-y')^{2/3}}\,dy' \quad (16)$$

$$\eta_c^* = \ln\frac{C_{M+n}^s}{C_{M+n}^b} + t_+\left(1 - \frac{C_{M+n}^s}{C_{M+n}^b}\right) \quad (17)$$

$$V_{corr}^* = \eta_a^* + \eta_c^* + \Phi_0^* \quad (19)$$

$$i_{M+n}^* = \frac{J}{\delta}\left(\frac{C_{M+n}^s}{C_{M+n}^b}\right)^\gamma \left[e^{\alpha_a(n/Z)\eta_a^*} - e^{-\alpha_c(n/Z)\eta_c^*}\right] \quad (18)$$

or

$$i_{M+n}^* = \frac{J}{\delta}\left(\frac{C_{M+n}^s}{C_{M+n}^b}\right)^\gamma \left[e^{\alpha_a(n/Z)\eta_a^*} - e^{-\alpha_c(n/Z)\eta_a^*}\right] \quad (18)$$

where $J = ZFr_0 i_0^b/RT\kappa$.

The voltage balance and zero net current conditions are:

$$V_{corr}^* = \eta_a^* + \eta_c^* + \Phi_0^* \quad (19)$$

$$\int_A i_{net}^* dA = 0 \quad (20)$$

The complete working equations are listed in Table 1, and the solution procedure has been discussed by Chiu and Selman [14].

2.2. *Results*

Figures 2–4 show the distribution of the anodic current density and the ohmic resistance at the surface of a corroding RHE as a function of the two parameters J and δ. In the application discussed here the concentration ratio of corrodant to metal ion is such that N is negligible.

Figure 2 shows that when the kinetics are very fast, i.e., $J \to \infty$, the current distribution for a fixed value of δ, i.e., constant rotation rate and ohmic resistance, approaches the cathodic current distribution at a sphere (dotted line). This differs from the current distribution of a non-corrosion electrode reaction at a RHE or RDE, which would approach the primary current distribution as $J \to \infty$. The difference is mainly due to the fact that the ohmic resistance is determined by i_{net} or $i_c + i_{M+n}$. In the present case, i_c has a fixed, non-uniform, distribution. As $J \to \infty$, i.e., the ohmic resistance becomes dominant over the kinetic resistance, the voltage balance equation requires that the net current distribution is uniform. In other words, the cathodic limiting current distribution serves also as the primary current distribution of the corrosion reaction at the RHE.

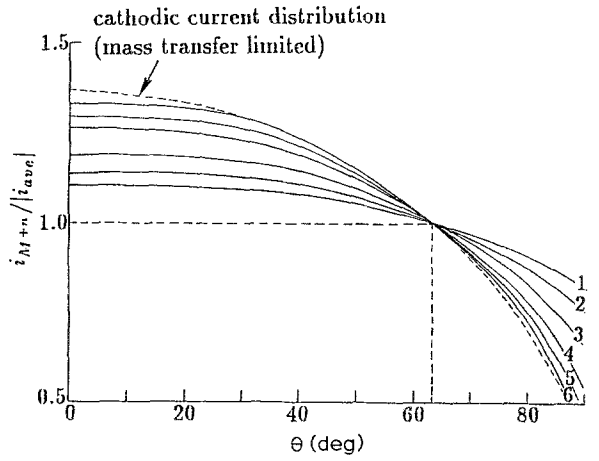

Fig. 2. Anodic current distribution at a corroding hemisphere as a function of polar angle θ. Variation of polarization parameter, J: (1) 0.5, (2) 1.0, (3) 2.0, (4) 5.0, (5) 10.0 and (6) 50.0. Other parameters: $\delta = 1$, $N = 0.01$, $\alpha = 0.5$ and $\gamma = 1$.

As shown in Fig. 3, for a fixed value of J but very high rotation rate ($\delta \to \infty$), the current distribution approaches likewise the cathodic limiting current distribution, since the ohmic resistance becomes again dominant, this time with respect to mass transfer resistance.

An unexpected and interesting feature observed in this limited parametric study is that to a good approximation, all curves intersect at $\theta = 62°$ where $i_{M+n}^* = 1$ and $IR = 0$ (see Fig. 4). In other words, the corrosion potential measured in such a corrosion system is representative of the average corrosion current density (provided N is small).

The errors incurred when one neglects the ohmic effect, are shown in Fig. 5 as functions of δ and J ($N = 0$, $\alpha_a = \alpha_c = 0.5$, $n = Z$, and $t_+ = 0$). The error is $1 - i_{M+n}^*$, where i_{M+n}^* is obtained by linear interpolation between finite difference values of θ such that Φ_0^* is equal to zero. As indicated in the figure, at a constant value of δ the error increases with decreasing

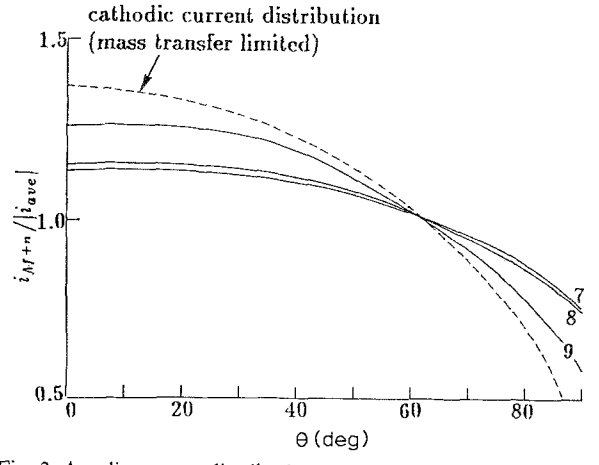

Fig. 3. Anodic current distribution at a corroding hemisphere as a function of polar angle θ. Variation of polarization parameter, δ: (7) 0.5, (8) 5.0 and (9) 20.0. Other parameters: $J = 1$, $N = 0.01$, $\alpha = 0.5$ and $\gamma = 1$.

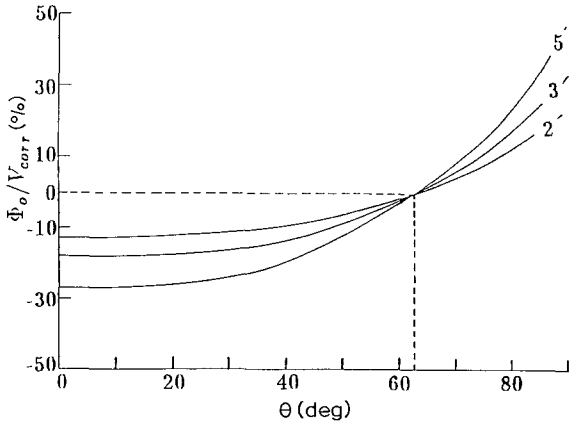

Fig. 4. Ohmic resistance distribution at a corroding hemisphere as a function of polar angle θ. Variation of the polarization parameter, J: (2) 1.0, (3) 2.0 and (5) 5.0. Other parameters: $\delta = 1$, $N = 0.01$, $\alpha = 0.5$ and $\gamma = 1$.

J but then approaches a limiting value. This limiting value depends on δ but in practice does not exceed 3%. In other words, if the level of ohmic resistance is fixed, the faster the kinetics of the metal dissolution reaction (large J), the smaller the IR contribution to the measured corrosion potential.

3. Kinetic parameters

3.1. *Test of the method*

To test the applicability of the method to a typical corrosion problem, a set of corrosion current-potential test data was synthesized by computer using $i_0^b = 6\,mA\,cm^{-2}$, $\alpha_a = 0.5$ and the constraint $\alpha_a + \alpha_c = 1$ ($n = Z$, $t_+ = 0$). A second set of data was generated using the same potential values, but with $\pm 5\%$ variation to test the sensitivity of the method to experimental error. A non-linear parameter estimation program, based on the simplex method [14, 15], was used to fit these sets of data.

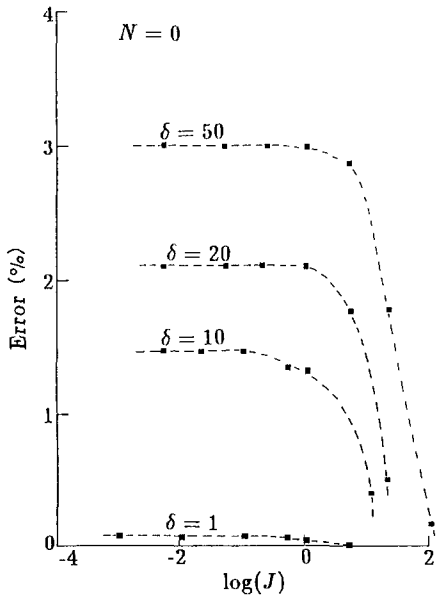

Fig. 5. Error in corrosion potential measurement due to ohmic resistance contribution at a corroding hemisphere. The polarization parameters J and δ are varied.

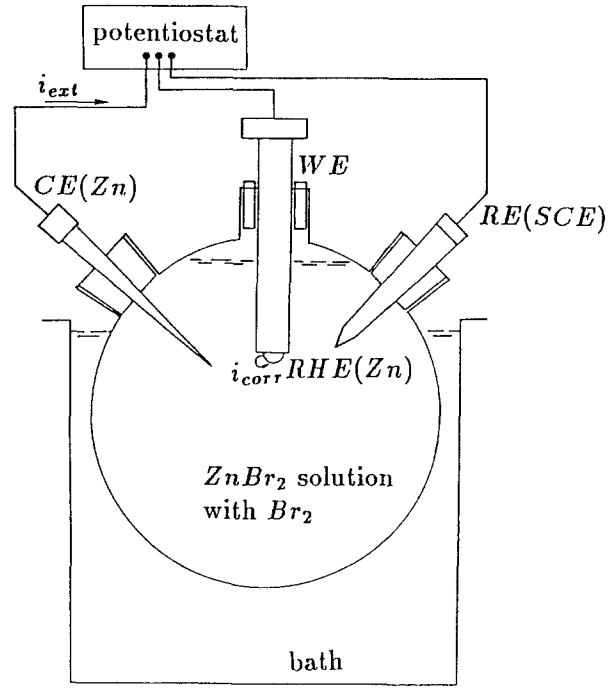

Fig. 6. Schematic of a RHE Cell for electrochemical measurements.

As shown in detail elsewhere [14, 16], the estimated parameters converge clearly to the actual data used. The errors incurred by neglecting the IR effect are, in the present case, estimated to be no more than 4%.

3.2. *Experimental data for the Zn/Br_2 system*

Corrosion potential-current data were collected for the zinc-bromine couple in solutions of $ZnBr_2$ and $ZnSO_4$. A RHE (Fig. 6) was used consisting of a

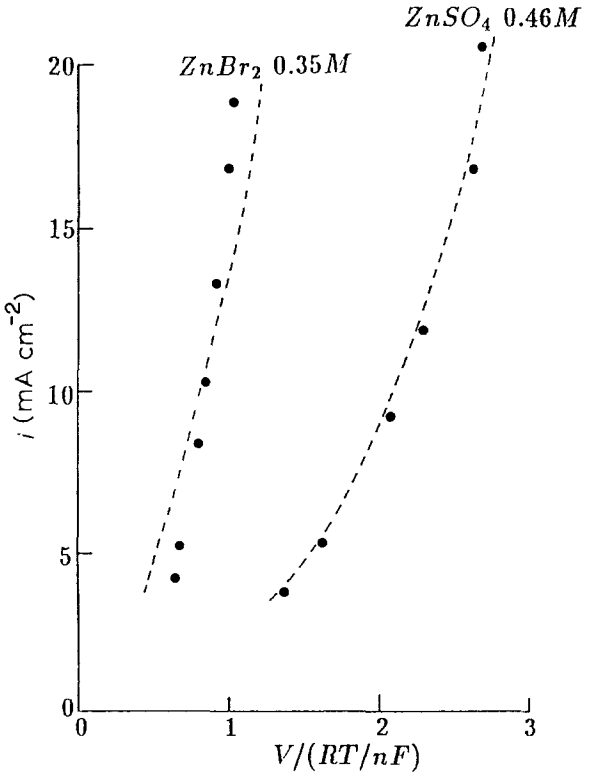

Fig. 7. Typical corrosion-current against potential response in $ZnBr_2$ and $ZnSO_4$ solutions (varying rotation rate and $ZnBr_2$ concentration). (●) Experimental values, (– – –) model prediction.

Table 2. Kinetic parameters of the mechanism (Equations 2 and 3) from corrosion potential measurements. The values in parentheses are obtained from the Allen-Hickling plot

	Concentration (M)	i_0^b ($mA\,cm^{-2}$)	α_a
$ZnBr_2$	0.05	1.59(0.92)	1.0(1.22)
	0.20	6.74(3.34)	1.0(1.44)
	0.35	8.59(1.17)	1.0(3.25)
$ZnSO_4$	0.46	1.43(1.05)	1.0(1.17)

zinc hemispherical electrode, 0.7–1.0 cm in diameter, attached to a Teflon cylindrical shaft of 2 cm in diameter. The RHE was immersed in approximately 3000 ml of a solution, containing 0.05–0.5 M $ZnBr_2$ or $ZnSO_4$ and 0–30 mM Br_2. Details of the experimental procedure are given in Chiu [16]. The fitting procedure described above was applied to these data. Typical experimental data and fitted curves are shown in Fig. 7. The optimal-fit values of the parameters i_0^b and α_a are tabulated in Table 2. Also shown in Table 2 (in parentheses) are the parameters obtained by linear regression of $\ln(i_{corr}/[1 - \exp(-(nF/RT)\eta_{corr})])$ against η_{corr}, i.e., the Allen-Hickling plot [13] of the corrosion potential and current density. The intercept of such a plot yields $\ln(i_0^b)$ and the slope, $(nF/RT)\alpha_a$.

The fit of the data in Fig. 7 appears at first sight acceptable. However, upon closer examination, a systematic deviation was observed, i.e., an overestimation of anodic potential at high i_{corr} and underestimation at low i_{corr}. The anomalous character of the fit in Fig. 7 is also evident from the findings that: (1) $\alpha_a = 1$ for all results obtained by the simplex method (under the constraints $\alpha_a + \alpha_c = 1$, α_a, $\alpha_c > 0$); and (2) $\alpha_a > 1$ for results calculated using the kinetic expression and the Allen-Hickling plot.

In order words, the corrosion mechanism of zinc by bromine cannot be adequately represented by a Butler-Volmer type of kinetic rate expression. Therefore, it was concluded that a further investigation of the mechanism was needed, and that the analysis might have to go beyond the traditional models leading to Butler-Volmer kinetics.

4. Alternative mechanisms involving chemical reaction steps

In a study of copper dissolution in oxygenated sulphuric acid solutions, Anderson *et al.* [17] proposed a mechanism which involves, in addition to electrochemical steps, a direct chemical reaction of oxygen with the Cu^+ intermediate. References to a similar mechanism applied to other system, e.g. aluminum dissolution in solutions containing halide, nitrate, etc., are also cited in their paper. Qualitatively, such a direct chemical reaction whose rate is independent of potential, gives rise to a rapid change in corrosion current while potential changes relatively little. This behaviour is very similar to that observed in Fig. 7.

In the case of zinc corrosion by bromine, it also seems desirable to explore the possibility of a corrosion mechanism including a chemical reaction step. There are additional arguments for such a mechanism. It has been reported by industrial developers of the zinc/bromine battery [18] that zinc deposited from weakly brominated solutions has a very different morphology from that in non-brominated solutions. In the presence of bromine, the tips of zinc protrusions tend to be flat rather than sharply pointed. This again suggests that the reaction follows a different reaction path than the conventional combination of Equations 2 and 3.

4.1. *Analysis of the corrosion mechanism*

The following reaction mechanism with parallel electrochemical and chemical reaction steps would be relatively simple and yet, as shown below, fit the data very well:

$$\text{electrochemical}\begin{cases} Br_2 + e^- \rightleftharpoons Br_{ad} + Br^- & (21a)\\ Br_{ad} + e^- \rightleftharpoons Br^- \quad \text{rds} & (21b)\\ Zn \rightleftharpoons Zn^* & (22a)\\ Zn^* \rightleftharpoons Zn^{+2} + 2e^- \quad \text{rds} & (22b)\end{cases}$$

$$\text{chemical}\begin{cases} Zn^* + 2Br_{ad} \overset{k'}{\rightleftharpoons} ZnBr_2^* \quad \text{rds} & (23a)\\ ZnBr_2^* \longrightarrow 2Br^- + Zn^{+2} & (23b)\end{cases}$$

where Zn* is the zinc-adatom. Assuming that the surface coverage of Zn* is small, the Zn* surface concentration can be expressed as $[Zn^*] = K$, where K is the equilibrium constant of Reaction 22a. If one further assumes that the reaction rate of Reaction 23b is fast, i.e., $[ZnBr_2^*] \approx 0$, then the backward reaction rate of Reaction 23a is small compared to the forward rate. From the above assumptions, the local bromine reaction rate may be expressed as

$$\begin{aligned} r_{Br_2} &= -k_c' C_{Br_{ad}} e^{-(1-\alpha)\phi^*} + k_a' C_{Br^-} e^{\alpha\phi^*} - k' K C_{Br_{ad}}^2 \\ &\approx -k_c C_{Br_{ad}} e^{-(1-\alpha)(\phi^* - \phi_e^*)} - k' K C_{Br_{ad}}^2 \\ &= -\frac{k_c}{\sqrt{(k)}} \Phi e^{-(1-\alpha)(\phi^* - \phi_e^*)} - \Phi^2 \end{aligned} \quad (24)$$

where the notation is as follows:

ϕ^* dimensionless electrode potential (normalized by $RT/2F$)
ϕ_e^* dimensionless equilibrium potential of zinc half reaction
Φ $\sqrt{(k)} C_{Br_{ad}} = \sqrt{k' K} C_{Br_{ad}}$
k' forward rate constant of chemical Reaction 23a
k_c $k_c' e^{-(1-\alpha)\phi_e}$
k_c' cathodic rate constant of Reaction 21b
α anodic transfer coefficient of Reaction 21b.

A second order rate expression in $C_{Br_{ad}}$ for the chemical reaction is used for Reaction 23a. Also, the term $k_a' C_{Br^-} e^{\alpha\phi^*}$ is neglected, because ϕ^* is a large negative number (≈ -100).

The local zinc reaction rate is expressed as:

$$i_{Zn^{+2}} = kC^2_{Br_{ad}} + i_0^b \left(\frac{C_{Zn^{+2}}}{C^b_{Zn^{+2}}}\right)^{\gamma} \times [e^{\beta(\phi^* - \phi_e^*)} - e^{-(1-\beta)(\phi^* - \phi_e^*)}] \quad (25)$$

Here the standard form of the Butler-Volmer equation is adopted for Reactions 22a and 22b, where γ and β refer specifically to zinc ions and zinc dissolution, respectively.

For a given corrosion potential, the current distribution of zinc dissolution and the average corrosion current can be determined, if the parameters $k_c/\sqrt{(k)}$, α, β, i_0^b and γ are known. Conversely, some of these parameters may be determined from corrosion potential measurements.

The same non-linear parameter estimation program used earlier in this paper is employed to extract from the experimental data (Fig. 7) two of the kinetics parameters, namely, $k_c/\sqrt{(k)}$ and i_0^b. In this analysis the transfer coefficients α, β and the reaction order γ are assumed to be 0.5, 0.5 and 1, respectively. The values of the kinetic parameters obtained are listed in Table 3.

The best fit of the corrosion potential-current data is also shown in Fig. 8. A much better fit is obtained than in the earlier attempt (Fig. 7).

The following conclusions may be drawn from this analysis:

1. The standard exchange current density of zinc dissolution in 1 M zinc solution is less than 20 mA cm^{-2} (scaling to 1 M based on the assumption of first-order kinetics). This is in mid-range of the literature data (some of the latter vary from 0.5 to 700 mA cm^{-2}; see Hsie [19] for a compilation of literature data).
2. Assuming typical values of the kinetic parameters, the ratio of chemical to electrochemical zinc corrosion by bromine in $ZnBr_2$ solutions is always large. This, however, is apparently not the case in uncomplexed solutions such as $ZnSO_4$.

From Table 3, it can be seen that the estimated i_0^b does not increase regularly with increasing Zn^{+2} concentration as expected. This inconsistency is primarily due to the strong interaction of the two parameters being estimated. Only the ratio of $k_c/\sqrt{(k)}$ and i_0^b

Table 3. Kinetic parameters of alternative reaction mechanism (Equations 21–23) obtained from corrosion potential measurements

	Concentration (M)	i_0^b ($mA\,cm^{-2}$)	$\frac{k_c}{\sqrt{k}}$ $(A\,cm^{-2})^{1/2}$	$i_0^b \Big/ \frac{k_c}{\sqrt{k}}$
$ZnBr_2$	0.05	1.0	$\frac{1}{13.42}$	13.42
	0.20	4.2	$\frac{1}{9.95}$	41.8
	0.35	0.5	$\frac{1}{155}$	77.5
$ZnSO_4$	0.46	2.3	$\frac{1}{3.6}$	8.29

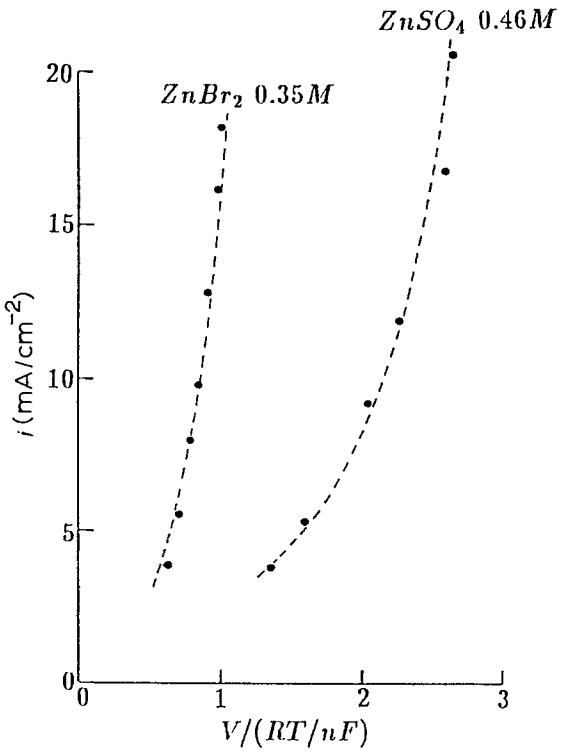

Fig. 8. Typical corrosion-current against potential response in $ZnBr_2$ and $ZnSO_4$ solutions, showing improved fit of predicted polarization. (●) Experimental values, (– – –) model prediction.

has reasonable accuracy. To clarify this, consider the ratio of chemical reaction rate to electrochemical rate, i.e., the ratio of the second term to the first term on the right-hand side of Equation 24:

$$\text{ratio} = \tfrac{1}{2}[-1 + \sqrt{(1 + 4r_{Br_2}[\sqrt{(k)}/k_c e^{(1-\alpha)(\phi^* - \phi_e^*)}]^2)}]$$

For typical values of the kinetic parameters (r_{Br_2} = 15 mA cm^{-2}, $k_c/\sqrt{(k)} = \sqrt{(1/200)}$ and $\phi^* - \phi_e^* = 1$), this *ratio* is around 2.4, i.e. about 70% of the zinc dissolution takes place through the chemical reaction path. In $ZnSO_4$ solution it is about 0.38 or only about 16% of that in $ZnBr_2$ solutions. In sulphate solutions, bromine is not complexed to form any Br_3^- ion, except at the electrode surface where Br^- is present as the corrosion product. Therefore, the smaller tendency toward chemical corrosion in these solutions suggests that the actual reacting species is Br_3^- instead of Br_2.

As evident from the small value of $k_c/\sqrt{(k)}$ for the case of 0.35 M $ZnBr_2$ solution, the chemical reaction rate is dominant. Comparing Equations 24 and 25, and assuming that $r_{Br_2} = i_{Zn^{+2}}$, one may write:

$$\frac{k_c}{\sqrt{k}}\sqrt{-r_{Br_2}}\,e^{-(1-\alpha)(nF/RT)(\phi^* - \phi_e^*)} = i_0^b \left(\frac{C_{Zn^{+2}}}{C^b_{Zn^{+2}}}\right)^{\gamma} \times [e^{\beta(\phi^* - \phi_e^*)} - e^{-(1-\beta)(\phi^* - \phi_e^*)}] \quad (26)$$

The strong interaction of parameters i_0^b and $(k_c/\sqrt{(k)})^2$, discussed in detail by Chiu and Selman [20], explains why only one parameter, $i_0^b/(k_c/\sqrt{k})$, can be estimated with reasonable accuracy.

The dominance of the chemical reaction path implies that even if the zinc electrode is under cathodic protection, the corrosion reaction still occurs at an

appreciable rate. This conclusion is confirmed by experimental observations, to be discussed below.

Therefore, the presence of bromine in the positive electrode compartment of a Zn/Br_2 cell indeed contributes to controlling dendrite formation, as has been from observations in the course of battery development [18]. Because the corrosion rate is highest in those areas of a microprofile where the mass transfer rate is highest, e.g. the tip of a protrusion, a levelling effect results.

4.2. *Verification of the proposed mechanism*

The RHE cell described earlier was used to check certain inferences from the above mechanism. Details of the experimetnal procedure are given in Chiu [16]. Two types of experiments were carried out: deposition mode experiments and dissolution mode experiments.

4.2.1. Deposition mode. If the corrosion of zinc by bromine is predominantly chemical in nature and independent of potential, certain rates of deposition at a RHE should result in a two-region pattern, one a deposition region and the other dissolution. The current distribution of zinc deposition along a RHE is more uniform than the distribution of the bromine flux, which is greatest at the pole. Therefore certain levels of net cathodic current result in deposition at the equator and dissolution in the pole region. This conclusion is illustrated by the results of computer modelling [14] shown in Fig. 9. It should be noted that the cathodic and anodic rate expressions of Equations 11 and 18 have been replaced by Equations 24 and 25. As the net zinc current increases (i.e., becomes more anodic), the boundary between the region of deposition and that of dissolution moves toward the equator. Note that this two-region pattern persists even at a net anodic average current (dissolution).

Shown in Fig. 10 are SEM photographs taken at different positions along the surface of a zinc RHE in bromine containing solution. The phenomenon described above is clearly observable. In the dissolution region traces of a needle-like deposit are also present.

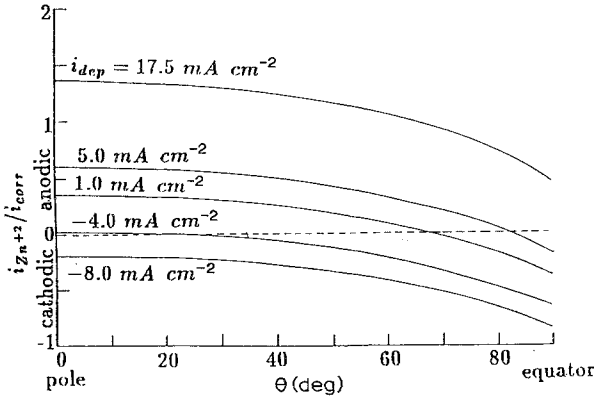

Fig. 9. Distribution of the zinc-ion flux (normalized as zinc current density with respect to the average corrosion current (density) along a rotating hemispherical electrode. $i_{corr} = 17.5\,mA\,cm^{-2}$, $k'/\sqrt{(k)} = 1/51$, $i = 1.2\,mA\,cm^{-2}$.

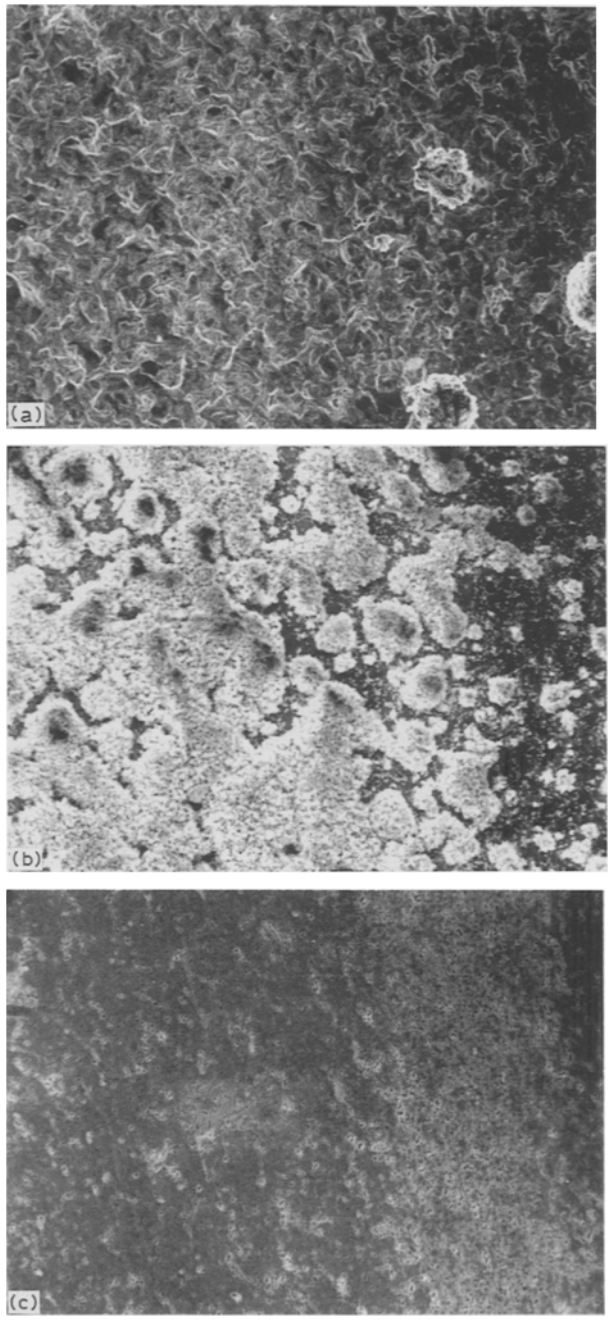

Fig. 10. SEM photographs of zinc deposited from 0.8 M brominated $ZnBr_2$ solution. The net deposition current density (determined by weight gain measurement) is $5\,mA\,cm^{-2}$, during 69 min. Experimental conditions: $C_{Br_2} = 30\,mM$, $\omega = 1000\,rpm$, pH = 5.1, magnification 200 × (a) at the equator of the RHE, (b) at about 30° from the pole, (c) at the pole.

A comparison of zinc deposit morphologies at high deposition current density, with and without bromine, is shown in Fig. 11. Chemical corrosion of zinc by bromine results in a much flatter deposit and smaller protrusions. The usual sharp tips of protrusions are completely absent.

4.2.2. Dissolution mode. In these experiments, the zinc electrode potential was controlled at a value more anodic than the corrosion potential. This causes the dissolution rate of zinc to be higher than the corrosion rate, which is given by Chin [6] and Newman [7]:

$$i_{corr} = 0.4508nFC_{Br_2}D^{2/3}\nu^{-1/6}\omega^{1/2} \qquad (27)$$

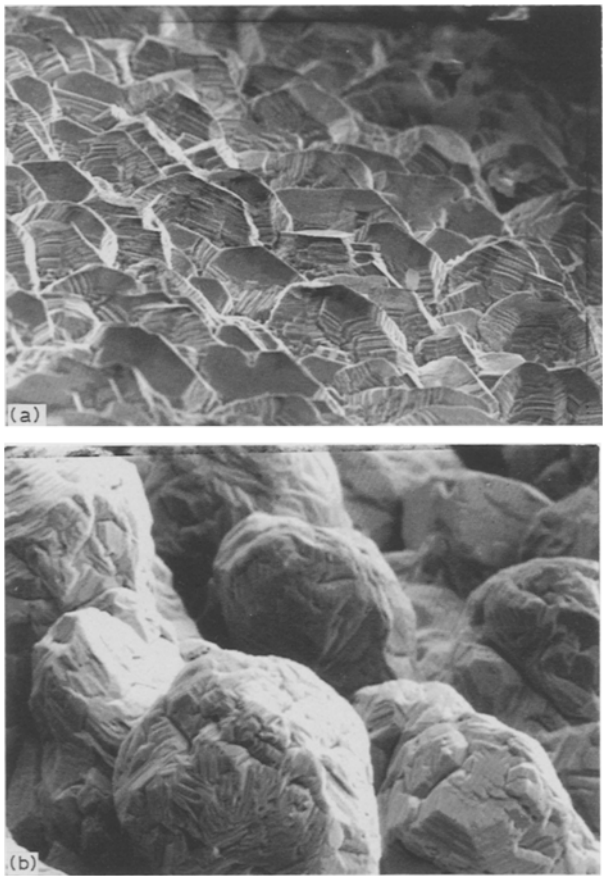

Fig. 11. SEM Photographs of zinc deposits at magnification 500×. The total loading for both pictures is approximately 70 mA h cm^{-2}. (a) $ZnBr_2$ = 0.2 M, ω = 1000 rpm, C_{Br_2} = 11.6 mM, pH = 2.9. (b) $ZnBr_2$ = 0.8 M, ω = 1000 rpm, C_{Br_2} = 0 mM, pH = 5.1.

Here C_{Br_2} and D pertain to bromine. The external currents for different rotation speeds were recorded and are shown in Fig. 12.

The solid line in Fig. 12 represents the total corrosion rate, calculated from Equation 27. The diffusivity used was obtained from Chiu and Selman [20]. Since the external current shows little variation with rotation speed, concentration and *IR* polarization will be practically constant. Therefore, the activation overpotential also is constant. According to conventional mixed potential theory, which considers only electrochemical reactions, the total dissolution rate, i.e., the sum of corrosion current and external current, under these conditions should have a fixed value. As is clear from Fig. 12, the experimental data contradict this. The discrepancy becomes understandable if only a very small portion of the corrosion rate (as determined from the bromine flux) contributes to the total current. This implies that most of the corrosion rate is potential independent, i.e., caused by a chemical reaction not involving the electrons, such as could take place between adsorbed atoms.

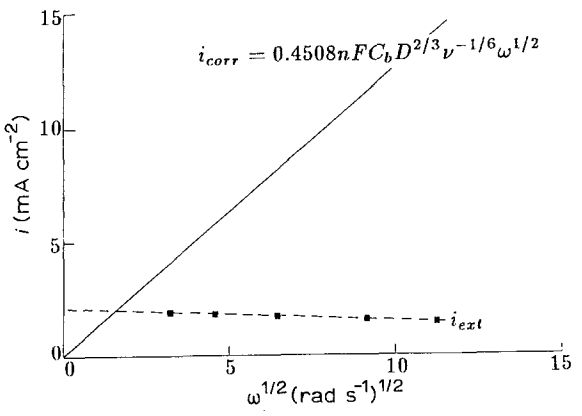

Fig. 12. Experimental results for i_{corr} and i_{ext}. The solution resistance was measured by the AC impedance method. C_{ZnBr_2} = 0.35 M, C_{Br_2} = 12.5 mM, E = −1.0 V/SCE and R_{soln} = 6 Ω.

5. Conclusions

The use of suitable corrosion couples to determine the electrode-kinetic reaction parameters of a fast electrode reaction has the obvious advantage of freedom from *IR* effect, compared to the conventional techniques (stationary and relaxation methods) which use a three electrode configuration. In the present work it is shown that for a wide range of mixed-control conditions (see Fig. 5), the error incurred by neglecting the ohmic effect is not more than 3%. Reasonably accurate estimates of the kinetic parameters (not more than 4% error in the cases studied) can be obtained using a kinetic expression such as the Butler-Volmer equation.

The Zn–Br_2 couple investigated in this paper showed unexpected mechanistic complications. The kinetic information obtained for the zinc dissolution reaction did not conform unambiguously to the classical (Butler-Volmer) type. A plausible explanation can be given if it is assumed that the dissolution mechanism of zinc in brominated solutions consists of parallel electrochemical and chemical reaction paths. In bromide solutions, where complexation of bromine with bromide ion to tri-bromide ion is appreciable, the chemical path is dominant over the electrochemical path. This is confirmed by deposition experiments at high current density (Fig. 11) and at variable flow rates (Fig. 12).

The chemical attack of bromine on zinc is effective in controlling dendrite formation. The higher the corrosion rate, the more effective it is against dendrites. However, as one would expect, it decreases the coulombic efficiency of a zinc/bromine cell. Therefore, a controlled leakage of dissolved bromine into the zinc electrode (NE) compartment of a battery may be optimal.

Acknowledgement

This project was supported by the Department of Energy through the Lawrence Berkeley Laboratory (Project No. 4 534 910).

References

[1] E. Gileadi, E. Kirowa-Eisner and J. Penciner, 'Interfacial Electrochemistry, An Experimental Approach,' Addision-Wesley, Reading, MA (1975).
[2] A. J. Bard and L. R. Faulkner, 'Electrochemical Methods

– Fundamentals and Applications,' John Wiley & Sons, New York (1980).
[3] G. P. Power and I. M. Ritchie, *Electrochim. Acta* **26** (1981) 1073.
[4] *Idem, ibid.* **27** (1982) 165.
[5] J. R. Scully, P. J. Moran and E. Gileadi, *J. Electrochem. Soc.* **133** (1986) 579.
[6] D. T. Chin, *ibid.* **118** (1971) 1434.
[7] J. Newman, *ibid.* **119** (1972) 69.
[8] K. Nisancioglu and J. Newman, *ibid.* **121** (1974) 241.
[9] N. Vahdat and J. Newman, *ibid.* **120** (1973) 1982.
[10] Exxon Research and Engineering Company, Linden, New York, 'Development of a Circulating Zinc-Bromine Battery,' Phase II-Final Report (1982).
[11] A. J. Bard (Ed.), 'Encyclopedia of Electrochemistry of the Elements,' Marcel Dekker, New York (1976).
[12] J. McBreen and E. Gannon, *J. Electrochem. Soc.* **133** (1986) 2047.
[13] J. Newman, 'Electrochemical Systems,' Prentice-Hall, Englewood Cliffs, NJ (1973).
[14] S. L. Chiu and J. R. Selman, 'Calculation of Corrosion Rate Distribution of a Rotating Metal Hemisphere,' AIChE Symposium Series, **83** (1987) 111.
[15] D. M. Himmelblau, 'Process Analysis by Statistical Methods,' Sterling Swift, Manchaca, Texas (1967).
[16] S. L. Chiu, 'Corrosion and Electrodeposition of Zinc in Flowing Acidic Solutions of Zinc Bromide,' Ph.D. Thesis, Illinois Institute of Technology, Chicago (1988).
[17] T. N. Anderson, M. H. Ghandehari and H. Eyring, *J. Electrochem. Soc.* **122** (1975) 1580.
[18] P. Grimes, Exxon Research and Engineering Company, Annandale, NJ, Private Communication (1983).
[19] W. C. Hsie, Ph.D. Thesis, Illinois Institute of Technology, Chicago (1985).
[20] S. L. Chiu and J. R. Selman, 'Corrosion of Zinc by Bromine under Flowing Conditions,' AIChE Symposium Series **83** (1987) 15.